Обзор ArXiv/astro-ph, 31 марта – 4 апреля 2025

От Сильченко О.К.

The dawn of disks: unveiling the turbulent ionised gas kinematics of the galaxy population at $z \sim 4-6$ with JWST/NIRCam grism spectroscopy

A. Lola Danhaive [1,2]★, Sandro Tacchella [1,2], Hannah Übler [3], Anna de Graaff [4], Eiichi Egami [5], Benjamin D. Johnson [6], Fengwu Sun [5], Santiago Arribas [7], Andrew J. Bunker [8], Stefano Carniani [9], Gareth C. Jones [1,2], Roberto Maiolino [1,2], William McClymont [1,2], Eleonora Parlanti [3,9], Charlotte Simmonds [1,2], Natalia C. Villanueva [10], William M. Baker [11], Daniel T. Jaffe[10], Daniel Eisenstein [6], Kevin Hainline [5], Jakob M. Helton [5], Zhiyuan Ji [5], Xiaojing Lin [12], Dávid Puskás [1,2], Marcia Rieke [5], Pierluigi Rinaldi [5], Brant Robertson [13], Jan Scholz [1,2], Christina C. Williams [14], Christopher N. A. Willmer [5]

Affiliations are listed at the end of the paper.

Accepted XXX. Received YYY; in original form ZZZ

ABSTRACT

Recent studies of gas kinematics at high redshift have reported disky systems which appear to challenge models of galaxy formation, but it is unclear whether they are representative of the underlying galaxy population. We present the first statistical sample of spatially resolved ionised gas kinematics at high redshift, comprised of 272 Hα emitters in GOODS-S and GOODS-N at redshifts $z \approx 3.9-6.5$, observed with JWST/NIRCam slitless spectroscopy and imaging from JADES, FRESCO and CONGRESS. The sample probes two orders of magnitude in stellar mass ($\log(M_\star[\mathrm{M}_\odot]) \approx 8-10$) and star formation rate (SFR $\approx 0.3-100\,M_\odot$/yr), and is representative down to $\log(M_\star[\mathrm{M}_\odot]) \approx 9$. Using a novel inference tool, GEKO, we model the grism data to measure morphological and kinematic properties of the ionised gas, as probed by Hα. Our results are consistent with a decrease of the rotational support v/σ_0 and increase of the velocity dispersion σ_0 with redshift, with $\sigma_0 \approx 100$ km/s and $v/\sigma_0 \approx 1-2$ at $z \approx 3.9-6.5$. We study the relations between σ_0, and v/σ_0, and different star formation tracers and find a large scatter and diversity, with the strongest correlations between σ_0 and SFR and SFR surface density. The fraction of rotationally supported systems ($v/\sigma_0 > 1$) slightly increases with cosmic time, from (36 ± 6)% to (41 ± 6)% from $z \sim 5.5$ to $z \sim 4.5$, for galaxies with masses $9 < \log(M_\star[\mathrm{M}_\odot]) < 10$. Overall, disks do not dominate the turbulent high-redshift galaxy population in the mass range probed by this work. When placed in the context of studies up to cosmic noon, our results are consistent with a significant increase of disk-like systems with cosmic time.

Наблюдения

Sample	N	S/N	$\lvert PA_{morph} \rvert$ [°]	r_e ["]	$\frac{v_{re}}{\Delta v_{re}}$	r_{obs}
Gold	41	> 20	< 60	> 0.12	> 1	-
Silver	132	> 10	< 75	> 0.12	> 1	-
Unresolved	99	> 10	< 75	-	-	-
Extended	80	> 10	< 75	> 0.12	> 1	> r_e

Table 1. Summary of the sub-samples defined in this work and their selection criteria. The extended sample is a sub-samble of the gold and silver samples. For each category, we report the number of galaxies N it contains, the S/N cut-off, the morphological position angle PA_{morph} cut-off, the size r_e requirement. We add constraints on whether the velocity gradient at r_e has to be resolved, $\frac{v_{re}}{\Delta v_{re}} > 1$, where where $\Delta v(r = r_e)$ is the 1σ lower limit, and constraints regarding the extent r_{obs} of the observed grism emission line map.

- JWSR/NIRgrism
- Разрешение ~1600
- Полоса F444W
- Поля GOODS (N&S)
- 272 H-alpha emitters
- 3.9<z<6.5
- Интервал масс log M_* : 8.0-10.0

Выборка

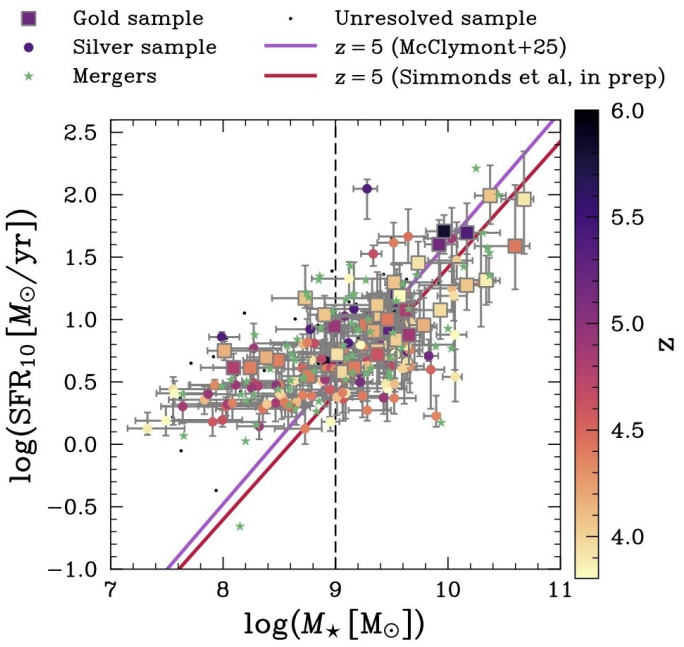

Figure 2. Star-formation rates (SFR_{10}) and stellar masses ($M_\star$) of our sample, derived with Prospector, colour-coded by the spectroscopic redshifts. The SFRs are averaged over 10 Myr. We compare our sample to SFMS prescriptions from McClymont et al. (2025a) and Simmonds et al (in prep.). Our sample is representative of the star-forming galaxy population at $M_\star > 10^9\ M_\odot$ (indicated by the vertical dashed line). Below this stellar mass, because our sample selection is based on S/N in Hα (Fig. 1), it is biased toward high SFRs relative to the SFMS. The discarded merger sample (green stars) is evenly spread across the parameter space and discarding it does not bias our results.

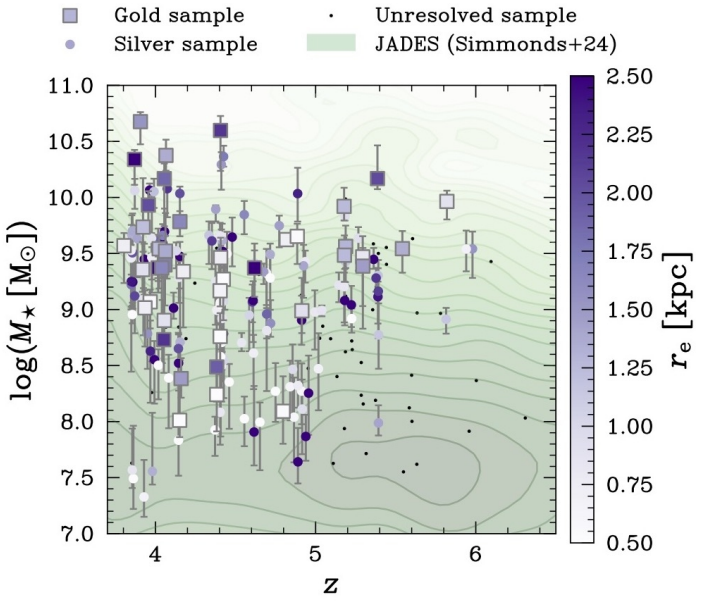

Figure 3. Distribution of our sample in the stellar mass ($M_\star$)-redshift plane. Our gold sample spans a wide range in stellar mass, but lies preferentially at $z < 5$. There are overall fewer galaxies at $z > 5$, with only few low mass systems ($M_\star \lesssim 10^9\ M_\odot$) falling in the gold and silver samples. Overall, our sample probes the high mass end of photometric candidates, as shown by the green contours representative of the JADES sample from Simmonds et al. (2024, and in prep), which is expected from our S/N cut. We colour-code galaxies in the gold and silver samples by their effective radius r_e in the rest-frame near-UV, highlighting that although more massive galaxies are typically larger, at fixed stellar mass, galaxies span a wide range of sizes.

Основной результат:

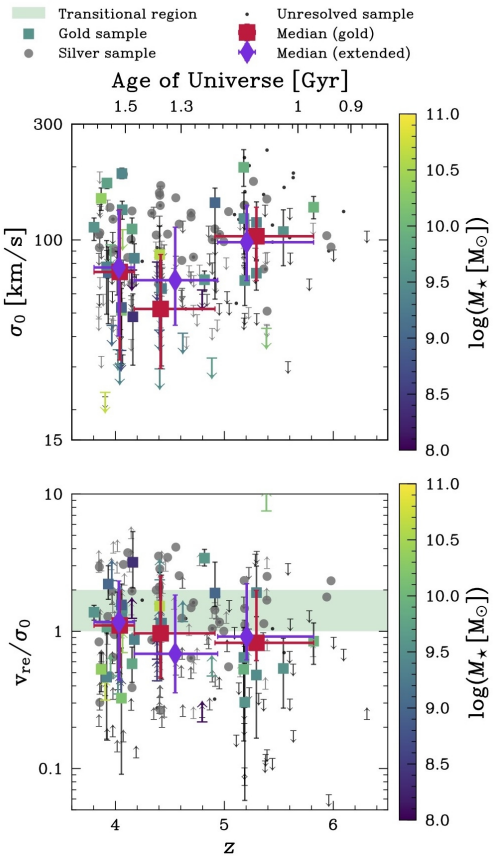

Figure 6. Redshift evolution of the intrinsic velocity dispersion σ_0 (top) and the rotational support v/σ_0 (bottom) for the Hα emitters in the gold sample (squares), silver (big circles), and unresolved (small dots) samples. The medians for the gold (red squares) and extended sample (purple diamonds), show a mild redshift evolution, for both σ_0 and v/σ_0, between $z \sim 4$ and $z \sim 6$. The errorbars on the medians represent the 16^{th} and 16^{th} quantiles along the y-axis, and the extent of the bin along the x-axis. Most of our sample lies in the dispersion supported regime ($v/\sigma_0 < 1$) and the transitional regions ($v/\sigma_0 = 1 - 2$; green shaded region), in part due to the high dispersions measured $\sigma_0 \approx 100$ km/s.

- Дисперсия скоростей теплого газа растет с красным смещением
- Степень поддержки диска вращением падает с красным смещением

Сравнение с литературой

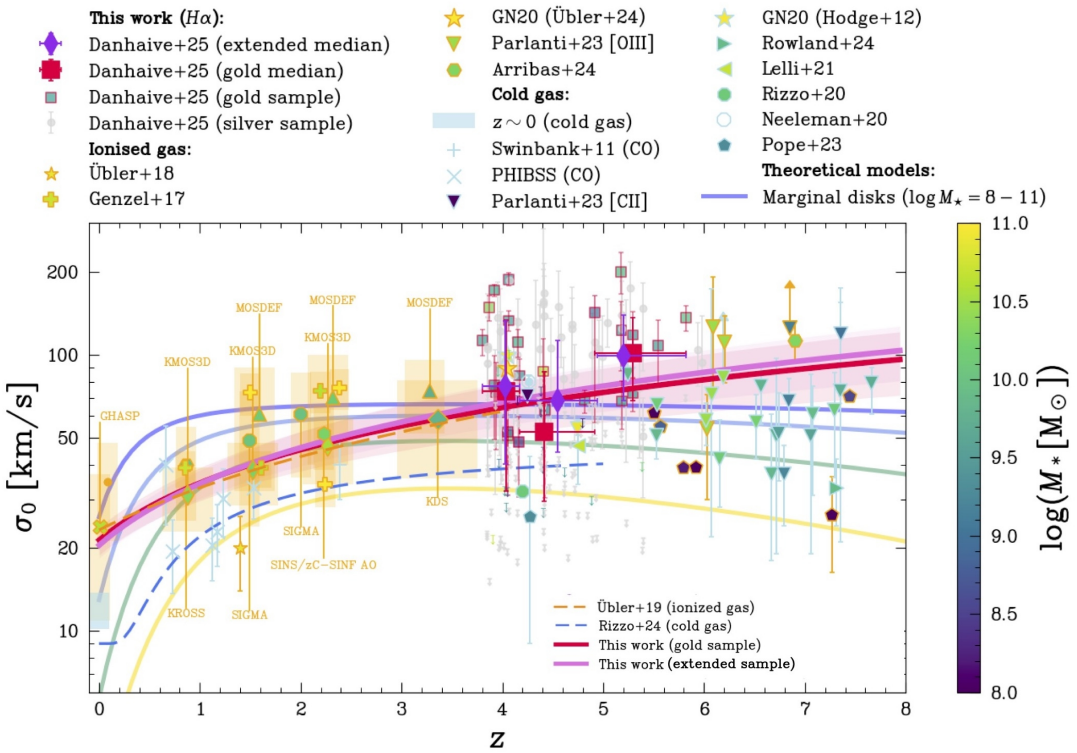

Figure 7. Intrinsic Hα velocity dispersion σ_0 as a function of redshift for our gold (red outlined squares) and silver (light gray circles) in the context of studies of warm ionised gas (i.e. Hα and [OIII]; orange outlines) and cold gas (i.e. HI, CO, and [CII]; blue outlines) kinematics across redshifts. The medians for the gold and extended samples are plotted in red squares and purple diamonds, respectively. The errorbars on the medians represent the 16th and 84th quantiles along the y-axis, and the extent of the bin along the x-axis. Our results are consistent with a decrease of σ_0 with cosmic time when compared to surveys from cosmic noon (KMOS3D Wisnioski et al. 2015, KROSS Johnson et al. 2018, MOSDEF Price et al. 2016, 2020, KDS Turner et al. 2017b,a, SIGMA Simons et al. 2016, SINS/zC-SINF Förster Schreiber et al. 2006, 2018, PHIBSS Tacconi et al. 2013, and points from Swinbank et al. 2011; Genzel et al. 2017) and the local Universe (GHASP Epinat et al. 2010, DYNAMO Green et al. 2014, EDGE-CALIFA Bolatto et al. 2017, HERACLES Leroy et al. 2009, THINGS Walter et al. 2008, and Dib et al. 2006; blue shaded region). Our best-fit relations (Eq. 8), with (purple) and without (red) including upper limits, agree with the fit from Übler et al. (2019) (light red - long dashes), which is defined out to $z \sim 4$. Similarly, we also include the exponential fit for cold gas measurements from Rizzo et al. (2024) (dark blue - long dashes) defined out to $z \sim 5$, which highlight a similar evolution of σ_0 tracing the cold gas, albeit with a factor 2-3 lower normalization. We compare our measurements with works at similar redshifts (Parlanti et al. 2023; Arribas et al. 2024; de Graaff et al. 2024a), as well as detection of dynamically cold systems at high-redshift Neeleman et al. (2020); Rizzo et al. (2020); Lelli et al. (2021); Pope et al. (2023); Rowland et al. (2024).

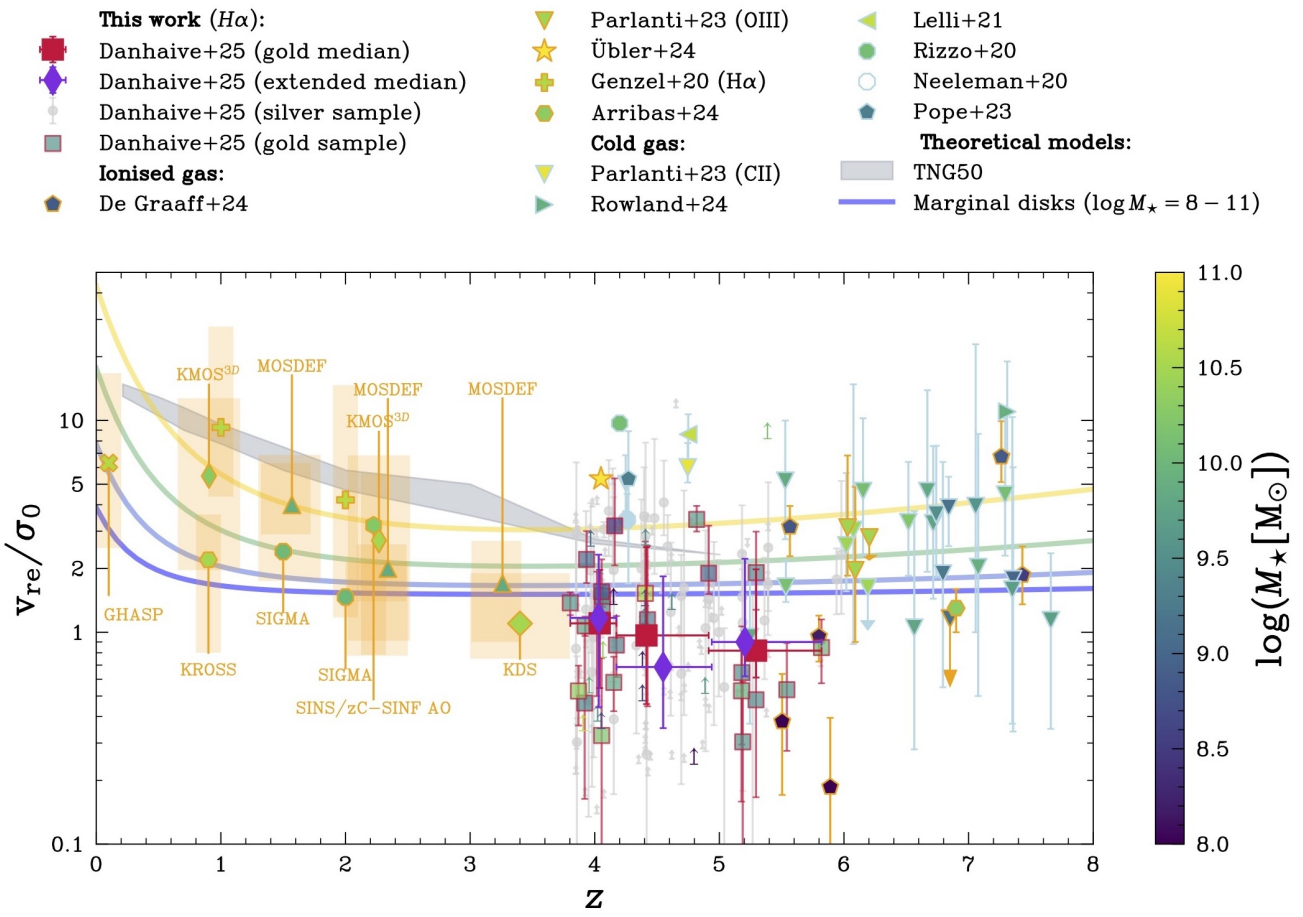

Figure 8. Evolution of the rotational support v/σ_0 with redshift for our gold (red outlined squares) and silver (light gray circles) in the context of studies of gas kinematics across redshifts. The medians for the gold and extended samples are plotted in red squares and purple diamonds, respectively. The errorbars on the medians represent the 16th and 16th quantiles along the y-axis, and the extent of the bin along the x-axis. All of our galaxies are $7 < \log M_\star[M_\odot] \lesssim 10$, and their kinematics are consistent with a decline of rotationally supported systems within our high-redshift sample, despite the presence of some rotation-supported systems (Fig. 6). They span similar v/σ_0 values as the ones of de Graaff et al. (2024a), despite probing slightly higher masses, and are overall consistent with cold gas ([CII]) measurements (blue outlines) from Parlanti et al. (2023), who find turbulent disks at $z \sim 6-7$. Our results are placed in the context of surveys (shaded orange regions) of ionised gas (orange outline) from cosmic noon and the local Universe: MOSDEF (Price et al. 2016), KMOS3D (Wisnioski et al. 2015), SIGMA (Simons et al. 2016), SINS/zC-SINF AO (Förster Schreiber et al. 2018), KROSS (Stott et al. 2016; Tiley et al. 2016), KDS (Turner et al. 2017b,a), and GHASP (Epinat et al. 2010). We also include medians from Genzel et al. (2020), and measurements from Übler et al. (2024). We add single-object detections of dynamically cold systems in the early Universe (Rizzo et al. 2020; Neeleman et al. 2020; Lelli et al. 2021; Pope et al. 2023; Rowland et al. 2024), which probe higher masses (i.e. more evolved systems) than our sample, and an unsettled disc in a protocluster (Arribas et al. 2024). Our measurements are consistent with a decrease of v/σ_0 with redshift as predicted by the TNG50 cosmological simulations (Pillepich et al. 2019), shown with the shaded gray region, and the Toomre (in)-stability model described in Wisnioski et al. (2011), indicated with solid lines. Within the context of lower-z measurements, our results are consistent with a decline of rotational support with redshift.

Всякие корреляции

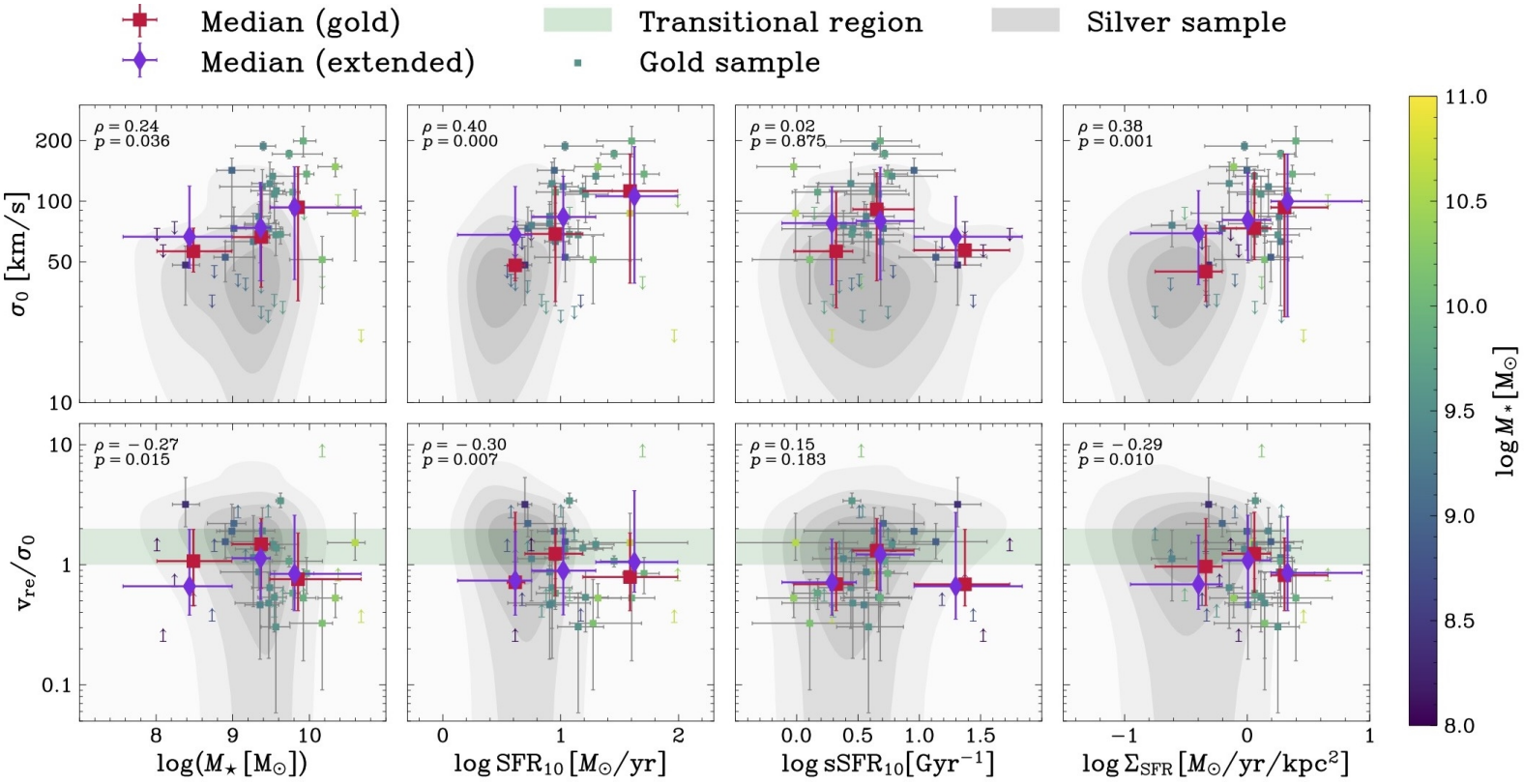

Figure 9. Dependence of the intrinsic velocity dispersion σ_0 (top panels) and rotational support v/σ_0 (bottom panels) on $M_\star$, SFR_{10}, $sSFR_{10}$, and SFR surface density $\Sigma_{SFR_{10}}$ for our gold (squares) and silver sample (gray contours). We find a significant correlation between σ_0 and SFR_{10}, which is highlighted by the running medians, for the gold sample (red squares) and for the extended sample (purple diamonds), and the Spearman rank coefficient ρ and p-value p for the resolved sample. The errorbars on the medians represent the 16^{th} and 84^{th} quantiles along the y-axis, and the extent of the bin along the x-axis. Both σ_0 and v/σ_0 show a (weaker) correlation with $\Sigma_{SFR_{10}}$, highlighting the role of surface density in efficiently driving turbulence in the gas. The trends with SFR_{10} and $\Sigma_{SFR_{10}}$ are stronger for σ_0 than v/σ_0, which could be caused by the fact that we probing many dispersion-supported systems ($v/\sigma_0 < 1$) and systems in the transitional regions (green shaded region) between dispersion and rotation support, where stable rotation has not yet been established.

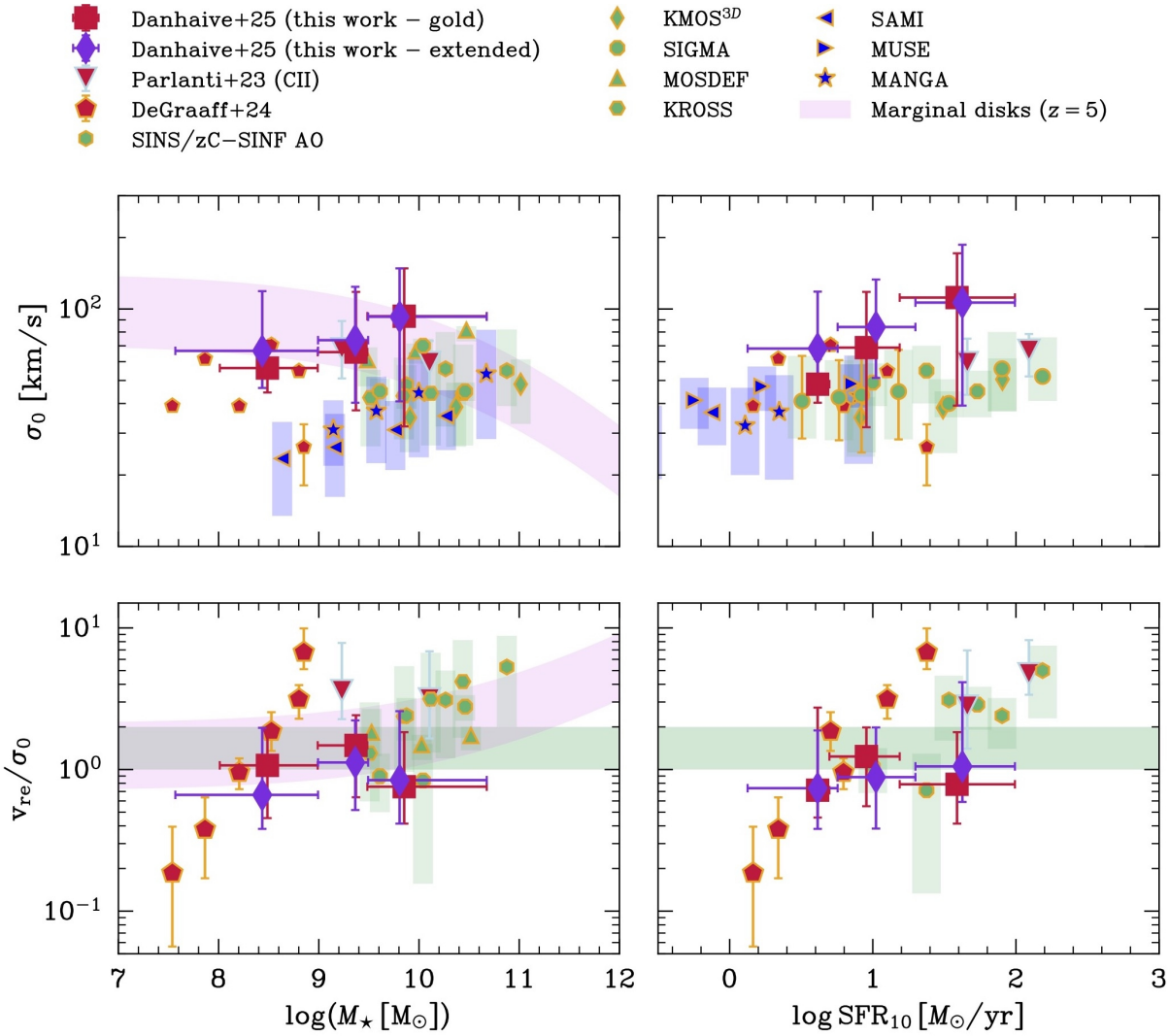

Figure 10. Dependence of σ_0 (top panels) and v/σ_0 (bottom panels) on stellar mass and SFR for our sample (red squares and purple diamonds) in the context of other high-redshift works (in red; Parlanti et al. 2023; de Graaff et al. 2024a), and works at cosmic noon (in green; see Fig. 7) and the local Universe (in blue; MANGA Yu et al. 2019, SAMI (Allen et al. 2015; Johnson et al. 2018; Green et al. 2018), and MUSE (Swinbank et al. 2017)). The errorbars on our plotted medians represent the 16th and 16th quantiles along the y-axis, and the extent of the bin along the x-axis. The σ_0-SFR relation holds across redshifts, for both ionised (Hα; orange outline) and cold ([CII]; blue outline) gas, although we find higher values of σ_0 and a steeper slope. Some works at lower redshift find a similar weak increasing trend for the $\sigma_0 - M_\star$ relation as our sample (Wisnioski et al. 2015; Förster Schreiber et al. 2018; Yu et al. 2019; Price et al. 2020), while Simons et al. (2017) finds no significant trend. The trends for v/σ_0 are less clear, but our results could indicate a flattening in the $v/\sigma_0 - M_\star$ relation at low masses $\log M_\star[\mathrm{M}_\odot] \lesssim 10$, which is consistent with other works in this mass range and which is predicted by the marginal disk model (purple shaded regions).

Эволюция с красным смещением

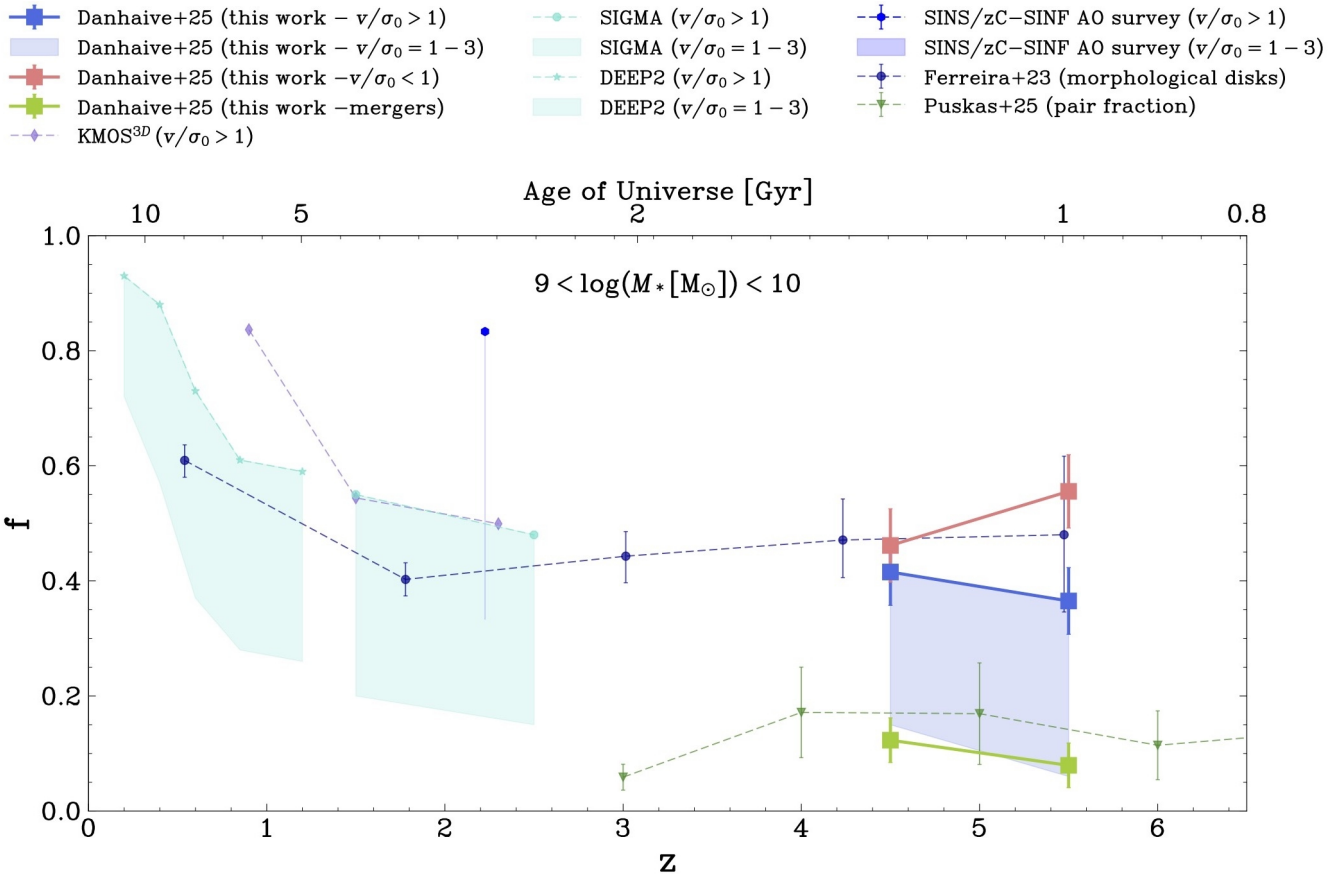

Figure 12. Evolution of the fraction of rotationally supported systems ($v/\sigma_0 > 1$) with redshift for our sample (blue lines) and for kinematic samples (Simons et al. 2017; Förster Schreiber et al. 2018; Wisnioski et al. 2019) and morphological sample (Ferreira et al. 2023) from the literature (blue dashed lines). We find a decrease in the fraction of systems with rotational support with redshift, consistent with predictions from lower redshifts, with fractions significantly lower if we consider a more conservative cut of $v/\sigma_0 > 1-3$ (blue shaded regions), with the lower edge at $v/\sigma_0 > 3$. This result contrasts the (on-average) constant fractions reported by Ferreira et al. (2023). We compare the fraction of pairs (green line), which we discard from our kinematic analysis, to the one reported in Puskás et al. (2025) (green dashed line), and find broadly consistent results.

Выводы

- В ранней Вселенной доминируют динамически горячие газовые диски
- Насколько они привязаны к ЗВЕЗДНЫМ дискам – один большой вопрос
- И наконец, остается без ответа вопрос: почему в МАССИВНЫХ галактиках со ВСПЫШКОЙ звездообразования – холодные диски, а на главной последовательности – горячие.